Desalination and Water Treatment
www.deswater.com

doi: 10.5004/dwt.2021.27053

224 (2021) 354–366
June

A comparative study: biological and chemical synthesis of iron oxide nanoparticles and their affinity towards adsorption of methylene blue dye

Doaa Mohamed Hammad*, Amany Ahmed Asaad

Central Laboratory for Environmental Quality Monitoring, National Water Research Center, Cairo, Egypt, Tel. +20 1012448984; email: doaahammad85@gmail.com (D.M. Hammad), Tel. +20 1027227409; email: amany_mahgob@hotmail.com

Received 16 June 2020; Accepted 11 January 2021

ABSTRACT

Biological synthesis of iron oxide nanomaterial using a water extract of *Chlorella vulgaris* microalga was carried out to investigate its efficiency in adsorbing methylene blue dye (MB) compared with another nanomaterial chemically prepared. Biologically synthesized FeO nanoparticles (BS-FeONPs) and chemically synthesized FeO nanoparticles (CS-FeONPs) were characterized by Brunauer–Emmett–Teller (BET) method, transmission electron microscopy (TEM) and X-ray diffraction (XRD). XRD patterns of both nanoparticles showed peaks of magnetite (Fe_3O_4), maghemite (Fe_2O_3) and wustite (FeO). BET analysis indicated that surface area and pore volume of BS-FeONPs were 85.705 m^2/g and 0.287 cm^3/g, respectively, with an average diameter of 44.770 Å. While in the case of CS-FeONPs, surface area, pore volume and mean diameter were 71.645 m^2/g, 0.32 cm^3/g and 90.744 Å, respectively. High-resolution TEM images showed that both nanomaterials formed cubic, spherical and irregular shapes with particle size of 4.8 nm in case of BS-FeONPs and 9.07 nm in the case of CS-FeONPs. Adsorption data for both BS-FeONPs and CS-FeONPs complies with Langmuir isotherm equation model (R^2 = 0.99) and the maximum adsorption amount (q_{max}) was 29.14 and 19.08 mg/g for BS-FeONPs and CS-FeONPs, respectively. Kinetic studies revealed that adsorption of MB is rapid and complies with the pseudo-second-order kinetic (R^2 > 0.99).

Keywords: Iron oxide nanoparticles; Chemical synthesis; Biosynthesis; *Chlorella vulgaris*

1. Introduction

Synthetic dyes are being utilized in different textile, cosmetics, leather, tannery, and food industries; it is water-soluble organic compounds complex in nature due to its aromatic structure, which make it much more stable to light, heat and oxidizing agents [1]. Approximately 15% of the dye stuff is estimated to be lost in industrial effluents during operations of manufacturing and processing [2–4]; this harmfully affects aquatic life by hindering the entry of light in water bodies, in addition, the majority of dyes are toxic and carcinogenic to human [5].

Recently biosorption has been evolved as an eco-friendly technique that was employed in dye removal from aqueous solutions; being of several advantages including simple design, easy operation, moreover, its high efficiency in removing different pollutants [6–10]. Several studies reported many biosorbents such as algae, bacteria, fungi and chitosan [5,8,9,11–13]. Microalgae are known to remove dyes by bioadsorption, biodegradation and bioconversion [14]; its biomass constitutes a diversity of functional groups including hydroxyl, carboxyl, phosphate, sulfate, and other charged groups that could be in charge of dye

* Corresponding author.

binding [12,15–17]. However, the majority of these groups are not accessible in the natural form of algae biomass. Therefore, the synthesis of nanoparticles from biomass of algae can be a better alternative to increase available biosorption sites of biomass. Also the latest progress in the nanotechnology field proved that ultra-fine biosorbents are a worthy substitute for dye removal [18,19]. Physical and chemical approaches are widely employed for the manufacture of metal and metal oxide nanoparticles; nevertheless, this manufacture involves the usage of highly reactive and toxic reducing agents that in turn cause undesired detrimental impacts on the environment, in addition some of these methods are expensive and labor intensive, requiring high temperature, vacuum and costly equipment. Researchers carry on hard work to develop facetious, effective and consistent green chemistry procedures for the assembly of nanomaterials. Several biological resources such as plants, algae, fungi and bacteria have been utilized for the fabrication of low-cost, energy-efficient, and nontoxic environmental friendly metallic nanoparticles [20–23].

Lately using algae for biological synthesis of nanoparticles has been investigated on a wide scale due to their availability and effectiveness [24–26]. Active biological molecules present in algae extracts have relatively been less subjected for nanoparticles synthesis compared with other natural sources including plants and bacteria [27,28]. Available functional groups and enzymes in cell walls of algae are acting as reducing agents, as a consequence of which reduction and fabrication of metal and metal oxide nanoparticles occur at ambient conditions [29,30]. Some examples of metal oxides nanomaterials used for dye removal are titanium dioxide (titania) [31], zinc oxide [32], magnesium oxide [33] and magnetic iron oxide [34].

Iron oxide (Fe_3O_4) magnetic nanoparticles have many applications in the field of environment because they have high saturation magnetization, biocompatibility, stability under ambient conditions and the simplicity of their preparation processes [35]. Green synthesis of iron nanoparticles has been reported from marine algae, brown algae [36,37], and red algae [38] and has been employed for bioremediation [37].

Several studies discussed the efficiency of dye removal by the green microalga *Chlorella vulgaris* natural biomass [1,8,14,39–41], other studies concerned with the effective removal of dyes by iron and iron oxide nanoparticles [42–48]; however, there are no studies up till now conducted to investigate the role of iron oxide nanoparticles synthesized by using *Chlorella vulgaris* microalga in the applications of dye removal from aqueous solutions; therefore the main objectives of the present study are: (1) biological synthesis of iron oxide nanoparticles using water extract of green microalga *Chlorella vulgaris*, (2) chemical synthesis of iron oxide nanoparticles, (3) characterization of both prepared nanomaterials, using Brunauer–Emmett–Teller (BET) analysis, transmission electron microscopy (TEM) and X-ray diffraction (XRD), (4) assessment of MB dye removal efficiency by both biological and chemical magnetic nanoparticles through a series of adsorption laboratory experiments, (5) description of adsorption mechanisms using Langmuir and Freundlich models, (6) recovery of biological and chemical iron oxide nanoparticles used in adsorption experiments and reexamining their adsorptive capacity for reuse in further applications of dye removal.

2. Materials and methods

2.1. Chemicals and materials

Iron chloride tetra hydrate ($FeCl_2{\cdot}4H_2O$), iron chloride hexa hydrate ($FeCl_3{\cdot}6H_2O$), methylene blue dye (99% purity), sodium hydroxide, hydrochloric acid (37%) and absolute ethanol (98%) were purchased from Sigma-Aldrich (Nottingham, UK). Green micro alga *Chlorella vulgaris* obtained as fine powder from Algae Biotechnology Unit, National Research Centre, Cairo, Egypt, where BG-II growth medium [49] was used for its growth. Deionized water was used to prepare all solutions.

2.2. Biological synthesis of iron oxide nanoparticles by using Chlorella vulgaris water extract

Standard methodologies described by several authors for biological synthesis of iron oxide nanoparticles were carried out with minor modifications [50,51]. 10 g of *C. vulgaris* fine powder was dissolved in 100 mL deionized water; chlorella water extract was heated to 60°C with stirring for 30 min at 900 rpm, and then centrifuged for 10 min at 1,500 rpm at room temperature. 60 mL of *C. vulgaris* water extract were added to a mixture of ferrous chloride (3.98 g) and ferric chloride (6.50 g), the solution was then kept on a magnetic stirrer at 1,000 rpm, during which sodium hydroxide solution (0.5 mol/L) was added drop wise until reaching pH 12 at which an intense black precipitate was formed indicating the synthesis of iron oxide nanoparticles. The precipitate formed was washed several times by deionized water until pH reached 7, then air-dried and finally ground to fine powder that was kept in a desiccator with few drops of ethanol (98% purity) to remove any moisture.

2.3. Chemical synthesis of iron oxide nanoparticles

60 mL of 0.1 mol/L hydrochloric acid (37%) was added to the previously mentioned mixture of ferrous and ferric chloride powder (as mentioned in section 2.2) instead of *C. vulgaris* water extract, the rest of the steps were the same as described in the biosynthesis of iron oxide nanoparticles by *C. vulgaris*.

2.4. Characterization of biologically synthesized and chemical synthesized iron oxide nanoparticles

The structural characterization of biologically and chemically synthesized iron oxide nanoparticles was investigated using BET method. The morphology and mean size of the samples were determined by TEM using JEOL-JEM 2100 at Central Laboratory of Petroleum Research Institute, Cairo, Egypt. Phase identification and structural analysis of the magnetic nanoparticles were carried out using XRD with the Cu-Kα radiation (λ = 1.5405 Å) in the 2-theta range from 10° to 70°.

2.5. Methylene Blue dye adsorption experiments

2.5.1. Determination of oxide nanoparticle dose

Methylene blue, (MB) a cationic dye, possesses a molecular formula of $C_{16}H_{18}N_3SCl$ and a molecular weight of

319.9 g/mol and colour index (CI) of 52015 [52]. MB dye stock solution of 25 mg/L concentration was prepared, and then different doses from 0.01 to 0.2 g were taken from BS-FeONPs and CS-FeONPs and added to 25 mL from MB dye stock solution with stirring at 300 rpm for 1 h to determine optimum dose at which highest removal efficiency occurred.

2.5.2. Effect of pH

25 mL from MB dye stock solution (25 mg/L) were used to study the effect of different pH values (1.5–12) on the adsorptive capacity of both BS-FeONPs and CS-FeONPs (at optimum dose). pH was adjusted by using 0.1 mol/L NaOH solution and 0.1 mol/L HCl, pH measures have been recorded using pH meter (Inolab WTW). All samples were stirred at 300 rpm for 1 h at room temperature.

2.5.3. pH zero-point charge (pH_{ZPC})

The pH zero point charge (pH_{ZPC}) of nanomaterials was measured by the electro-chemical method reported by Altenor et al. [6]. 50 mL of 0.01 mol/L NaCl solution was poured in 100 mL Erlenmeyer flasks, then the pH was first adjusted to successive initial values between 1.1 and 12 by using either NaOH or HCl (0.1 mol/L), and 0.15 g of orange peel was added to the solutions. After 48 h contact time, final pH was measured and plotted against the initial pH. The pH at which the curve crosses the line (pH final = pH initial) is taken as the pH of the pH_{ZPC}.

2.5.4. Effect of initial dye concentration

The effect of MB dye concentration on colour removal efficiency by both BS-FeONPs and CS-FeONPs (at optimum dose) was studied in the range of 10–50 mg/L dye solution concentration, with stirring at 300 rpm for 1 h at room temperature.

The amount of adsorbed dye at equilibrium, q_e, and dye removal efficiency were calculated from the following mass balance equations:

$$q_e = \frac{V}{M} \times \left(C_0 - C_e\right) \tag{1}$$

$$R_e = \frac{C_0 - C_e}{C_0} \times 100 \tag{2}$$

where C_e and C_0 are the equilibrium and initial concentrations of dye (mg/L); q_e is the equilibrium dye concentration on adsorbent (mg/g), V is the volume of dye solution (L), M is the mass of FeONPs sample used (g) and R_e is the removal efficiency [6]. The effect of adsorbent dosage was studied by varying the amount of FeONPs from 0.01 to 0.2 g. All of the adsorption experiments were performed by agitation at 300 rpm at 25°C ± 0.5°C and the average of three replicates experiments were reported.

2.5.5. Effect of contact time

Adsorption of MB dye by both biological and chemical synthesized iron oxide nanoparticles at optimum dose was monitored with increase in contact time from 30 to 120 min. Examined samples were stirred at 300 rpm at room temperature.

2.6. Recovery and reuse of iron oxide nanoparticles

Recovery of iron oxide nanoparticles was done by collecting nanoparticles used in different experiments and keeping them in 0.1 mol/L HCl solution for 24 h to purify the material, after which the material was washed several times with deionized water and then dried to be reused again in further adsorption experiments.

3. Results and discussion

3.1. Characterization of synthesized magnetic nanoparticles

Both biological and chemical synthesized iron oxide nanoparticles were studied for their structures as follows:

3.1.1. X-ray diffraction

Phase identification and crystalline structures of biological and chemical synthesized iron oxide nanoparticles were characterized by XRD as seen in Figs. 1 and 2. Since both BS-FeONPs and CS-FeONPs prepared from a mixture of ferrous and ferric chloride powder, their XRD patterns showed the presence of three crystalline phases; magnetite (Fe_3O_4), reference code 00-003-0863, maghemite (γ-Fe_2O_3), reference code 00-004-0755 and wustite (FeO), reference code 00-006-0615. Similar results obtained by a number of studies concerned with green and chemical synthesis of iron oxide nanoparticles [23,45,53–57]. The three most available formulas of iron oxides in nature are magnetite (Fe_3O_4), maghemite (γ-Fe_2O_3), and hematite (α-Fe_2O_3); these oxides considered to be very significant in the field of magnetic nanoparticles especially magnetite and maghemite since their biocompatibility has been proven by a number of studies, during manufacturing, the simultaneity of Fe_3O_4 and γ-Fe_2O_3 could be returned to the oxidation of magnetite to maghemite [58–60]. Magnetic nanoparticles possessing a magnetite or maghemite core chemistry have been used in solving numerous environmental complications; for example, they have been utilized in wastewater remediation through removal of heavy metals, salts, alkalinity, hardness and organic compounds; this is because of simplicity of manufacturing, easy optimization of their size and morphology and fast magnetic separation when exposed to external magnetic field [61,62].

3.1.2. BET analysis

BET analysis represented in Table 1 shows that the BET surface area and pore volume of biological synthesized iron oxide nanoparticles (BS-FeONPs) were 85.705 m^2/g and 0.287 cm^3/g, respectively, with an average diameter of 44.770 Å. On the other side, BET surface area, pore volume and mean diameter of chemical synthesized iron oxide nanoparticles (CS-FeONPs) were 71.645 m^2/g, 0.32 cm^3/g and 90.744 Å, respectively; BET results revealing the higher reactivity of BS-FeONPs towards adsorption and removal

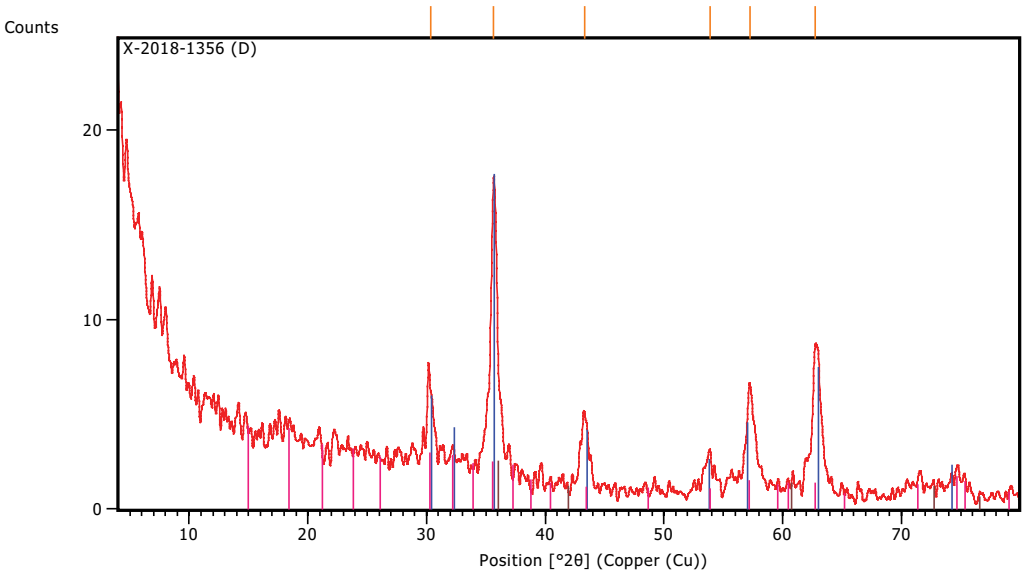

Fig. 1. XRD pattern of BS-FeONPs.

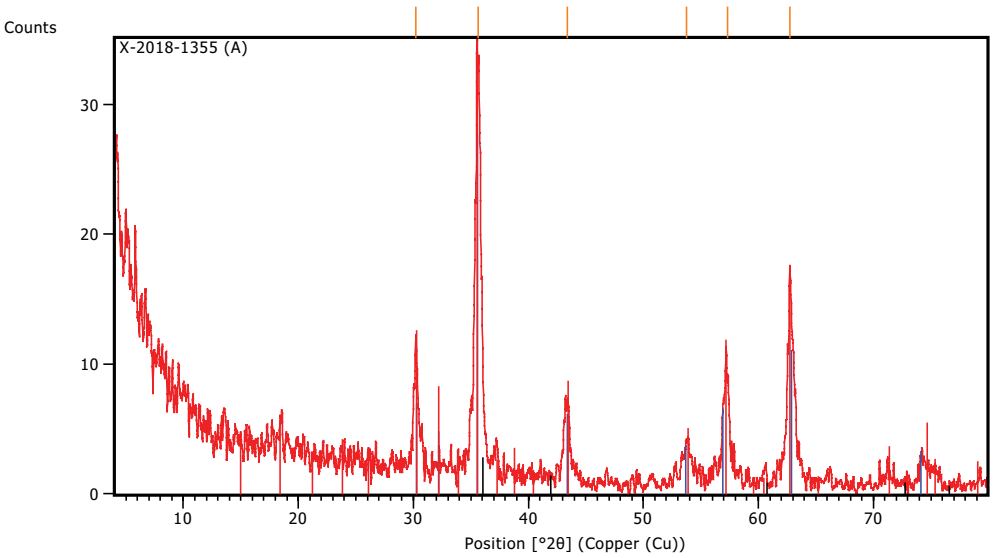

Fig. 2. XRD pattern of CS-FeONPs.

Table 1
Brunauer–Emmett–Teller parameters of BS-FeONPs and CS-FeONPs

Sample	Surface area m^2/g	Pore volume cm^3/g	Mean diameter Å
BS-FeONPs	85.705	0.287	44.770
CS-FeONPs	71.645	0.320	90.744

of MB dye from aqueous solutions; in this aspect, the green biosynthesis of iron oxide nanoparticles in addition of being simple and fast manufacturing procedure, economic and less waste production, it can also offer improved features, such as greater biocompatibility and biodegradability when compared with physical and chemical produced nanoparticles, this could be attributed to the occurrence of phytochemicals, which are compounds produced by plant itself, including flavonoids, xanthophyll, carotenoids, anthocyanin and phenolic acids, which are believed to participate in nanoparticles synthesis, acting as metal-reducing agents and capping agents to achieve a robust coating on the metallic nanoparticles [55].

3.1.3. TEM analysis

High resolution TEM images (HR-TEM) in Figs. 3 and 4 show that both synthesized FeONPs tend to form cubic, spherical and irregular shapes in form of clusters with particle size 4.8 nm in case of BS-FeONPs and 9.07 nm for CS-FeONPs; TEM results also indicated that particle size of both prepared nano materials was within the critical size for super paramagnetic iron oxide nanoparticles (SPIONs), which are known to be below 20 nm [63]. The smaller particle size of BS-FeONPs suggesting them to be more reactive than CS-FeONPs since they provide larger surface area for the reaction to occur [64] where higher biosorption sites on the surface were available for dye binding, according to Aksu [7], the biosorption is directly related with surface area of biosorbent, therefore the size of nanoparticles is one of the key factors that enforce the biosorption capability. Similar to our HR-TEM results [45] produced iron oxide nanoparticles in the form of irregular clusters when using extracts of green tea leaves (GT-FeONPs) to be used as Fenton-like catalyst for degrading aqueous anionic and cationic dyes. In agreement with previous studies [51] obtained iron oxide nanoparticles with multiple shapes, including square, needle and sphere when utilizing algae in synthesis of iron oxide nanoparticles to be applied in dye removal studies. The biosynthesis of iron oxide nanoparticles by reduction of ferric chloride solution with the macro alga *Sargassum muticum* studied by Mahdavi et al. [36]; they concluded that major components including sulphate, hydroxyl and aldehyde groups present in *Sargassum muticum* might result in the reduction of Fe^{3+} and stabilize the nanoparticles, Fe_3O_4-NPs produced were cubic in shape with particle size 18 ± 4 nm. In the same trend [65], used leaves of Andean blackberry, known also as *Rubus glaucus* Benth, to synthesize FeONPs, produced Fe_3O_4-NPs were found to have spherical shape with an aggregating nature and their size ranged from 40 to 70 nm; they suggested that polyphenolic compounds occurred in leaf extract are mostly accounting to the development of clusters and aggregation of the nanoparticles that acting as capping and stabilizing agents, they used the synthesized Fe_3O_4-NPs as an effective photo catalyst for the degradation of congo red, methylene orange and methylene blue dyes. Subramaniyam et al. [66] synthesized iron nanoparticles by using green microalga *Chlorococcum* sp. with iron chloride, the produced nanoparticles were found to have spherical shape with size ranging from 20 to 50 nm as determined by TEM; they predicted that biological molecules such as carbonyl and amine involved in polysaccharides and glycoproteins exist in algal cells were incorporated in the production of iron nanoparticles, which was proved by FTIR analysis. It was confirmed that both morphology and size of iron nanoparticles could be changed by changing the concentrations of extract and also the type of iron salt [67].

3.2. Adsorption experiments

3.2.1. Determination of optimum dose

Results presented in Table 2 and illustrated by Fig. 5 show an increase in the uptake percentage of MB dye from its solution with increasing dose concentration of both biologically and chemically synthesized FeONPs from 0.01 to 0.1 g after which the increase in dose concentration has no effect on decolorization percentage. Therefore, optimum dose for both nanomaterials was determined as 0.1 g/25 mL of MB dye stock solution which corresponds to 4 g/L at which maximum dye removal efficiency was attained by BS-FeONPs (99% removal) and CS-FeONPs (94% removal). All adsorption experiments (effect of time, pH and dye concentration) in addition to recovery experiments were carried out at optimum dose.

3.2.2. Effect of contact time

Data presented in Fig. 6 show that there was a gradual increase in dye removal efficiency by both synthesized nanomaterials with increasing contact time where

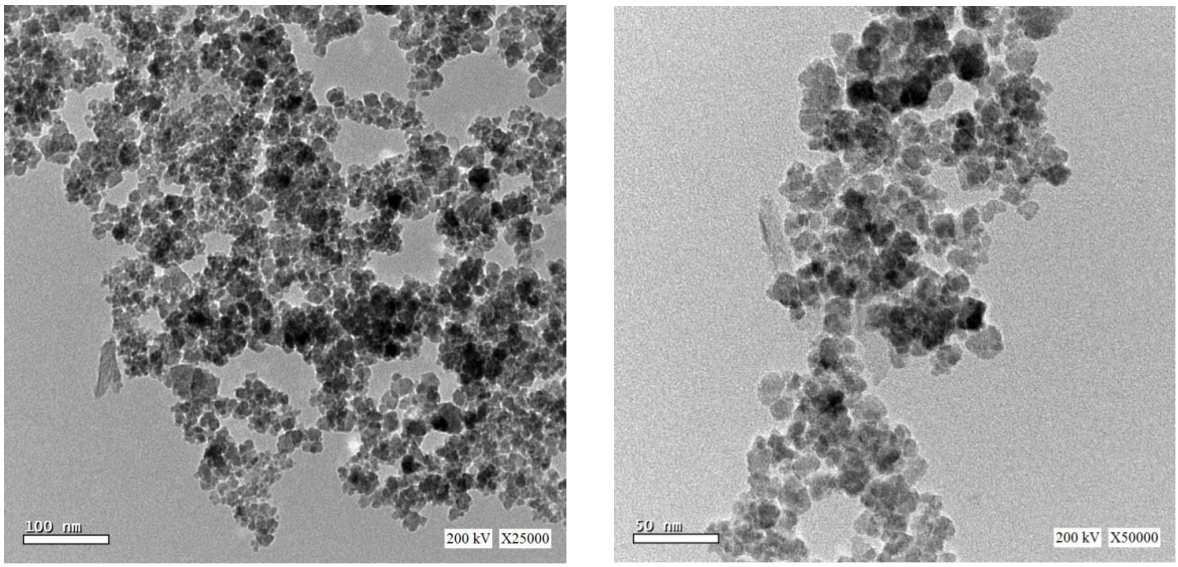

Fig. 3. TEM images of BS-FeONPs.

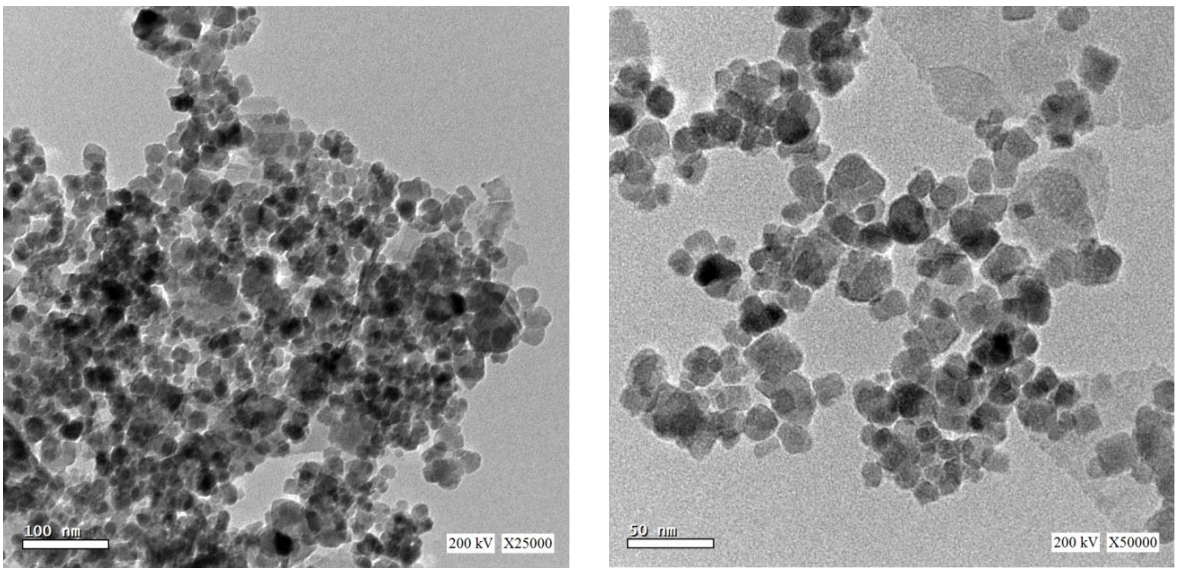

Fig. 4. TEM images of CS-FeONPs.

Table 2
Iron oxide nanoparticles optimum dose removal efficiency

Doses of iron oxide nanoparticles (g)	0.01	0.05	0.1	0.15	0.2
BS-FeONPs removal efficiency	85%	92%	99%	99%	99%
CS-FeONPs removal efficiency	80%	85%	94%	94%	94%

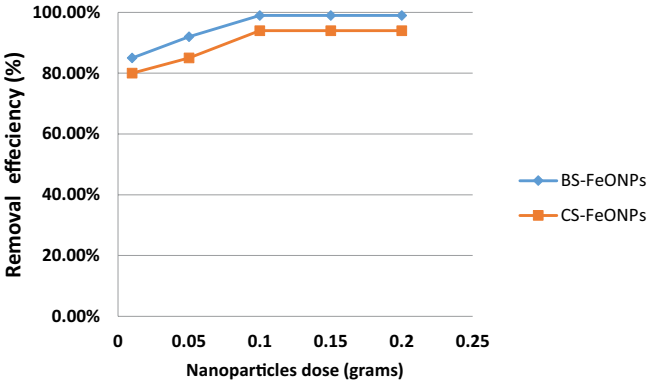

Fig. 5. Iron oxide nanoparticles optimum dose.

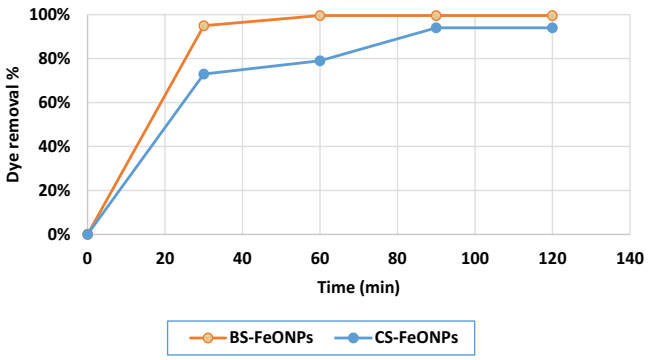

Fig. 6. Effect of contact time on dye removal by BS-FeONPs and CS-FeONPs.

adsorption of MB onto BS-FeONPs reached equilibrium within 60 min at which 99.6% removal was attained, on the other side of equilibrium was reached by CS-FeONPs after 90 min time of contact with 94% removal. Contact time is a major factor that influence removal efficiency, and most of the adsorption takes place in the first half hour and then the increase becomes very slowly [68]; this is particularly true and in conformity with our findings where 95% and 73% of MB dye adsorbed from its solution on BS-FeONPs and CS-FeONPs, respectively, after 30 min contact time. Data also indicated faster separation of MB dye from aqueous solution by BS-FeONPs when compared with CS-FeONPs, which could be attributed to increased active sites for dye binding on biological synthesized nanomaterial as a result of larger surface area leading to faster equilibrium [69]. In accordance with our findings, Rahimi [68] investigated the variation of contact time (0–120 min) on the removal of methylene blue from wastewater by adsorption onto $ZnCl_2$ activated corn husk carbon; they found that adsorption of MB reached equilibrium in 80 min, and explained that during adsorption the MB molecules at the beginning reach the boundary layer, then the molecules have to diffuse through the adsorbent surface and lastly diffuse into the porous structure of the adsorbent, this is why this phenomenon takes comparatively lengthier contact time [70].

3.2.3. Effect of pH

Variation in pH values is one of the most significant factors affecting dye adsorption onto suspended particles [71], where pH of aqueous solutions found to exert high influence on the sorptive uptake of dyes due to its impact on surface binding sites of the sorbent. The effect of pH of dye solution on the adsorptive capacity of both synthesized nanoparticles was investigated at pH range from 1.5 to 12. Fig. 7 shows that the adsorptive capacity of BS-FeONPs increased with increasing found that the increase in pH of solution, increases number of hydroxyl groups, therefore increasing number of negatively charged sites and enlarges the attraction between the cationic dye and surface of adsorbent, on the other side at lower pH the material surface charge might acquire positive charge, thus making (H^+) ions that race with dye cations causing a reduction in the quantity of dye adsorbed pH values from 1.5 to 7 where 100% removal efficiency was observed at pH 7, which lies in the pH range of most raw water (6.5–8.5) as mentioned in a study by Ruana et al. [72]. While in case of CS-FeONPs maximum removal efficiency (96%) was attained at pH 10; this could be explained in light of the following authors observations; Fil et al. [73] found that the increase in pH of solution, increases number of hydroxyl groups; therefore, increasing number of negatively charged sites and enlarging the attraction between the cationic dye and surface of adsorbent, on the other side at lower pH the material surface charge might acquire positive charge, thus making (H^+) ions that race with dye cations causing a reduction in the quantity of dye adsorbed [74]. Similarly, Özdemir et al. [75] mentioned that when a basic dye is dissolved in water, it tends to give positively charged ions, thus in acidic medium positively charged surface of sorbent inclines to oppose the adsorption of cationic sorbate species, while when pH of dye solution increases, the material surface tends to gain negative charge, thus causing an increase in dye adsorption due to increasing electrostatic attraction between positively charged sorbate and negatively charged sorbent. In agreement with our results, Boumediene et al. [76] found that the amount of methylene blue adsorbed at equilibrium on orange peel increased from 44,90 to 98,767 mg/g with increasing initial pH of solution from 3 to 9.

3.2.3.1. pH zero-point charge (pH_{ZPC}) measurements

pH_{ZPC} is an important adsorbent characteristic, as it determines the point of pH at which the surface of adsorbent has no net electrical charge. It was stated that at any scale of pH below pH_{ZPC}, the surface charge is positive; whereas, at pH level above pH_{ZPC}, the surface charge is negative [6]. Thus, this parameter has significant effect on the adsorption process. The pH_{ZPC} has been deduced from graphs where the initial pH is equal to the final pH (intersection of curves). The removal of MB dye is favorable when pH > pH_{ZPC} and it can be derived that the rise of aqueous pH to a higher scale than that of adsorbent pH_{ZPC} may lead to the increase of ionizable charge sites on the BS-FeONPs and CS-FeONPs surfaces.

At pH > pH_{ZPC} = 8.0 for BS-FeONPs and at pH > pH_{ZPC} = 7.8 for CS-FeONPs so the surface charges of BS-FeONPs and CS-FeONPs are negative. Several studies showed that MB has a positive charge in aqueous solutions; on the other hand, the increase of pH in aqueous solutions to higher than pH_{ZPC} leads to the increase of negative charge density on adsorbent surfaces, resulting in an increase of MB dye adsorption. As shown in Figs. 8 and 9, at any point of pH level above pH_{ZPC}, the adsorption of dye is higher than in other points. This phenomenon may be correlated to electrostatic interactions that appear between positive and negative charges of MB species and adsorbent surface, respectively.

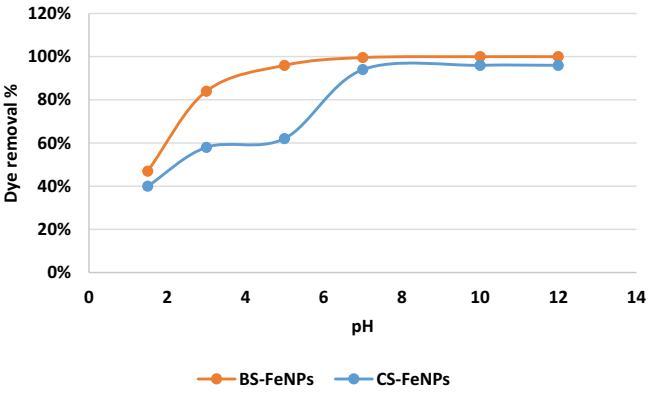

Fig. 7. Effect of pH values on MB dye removal by BS-FeONPs and CS-FeONPs.

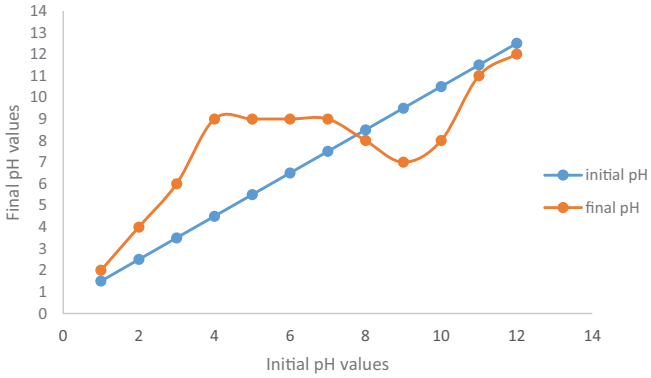

Fig. 8. pH_{ZPC} measurements for BS-FeONPs.

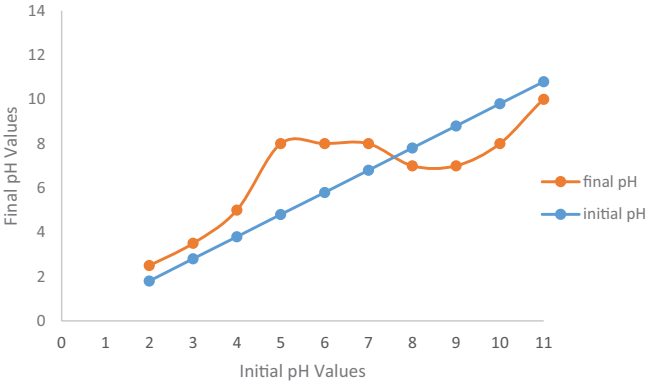

Fig. 9. pH_{ZPC} measurements for CS-FeONPs.

3.2.4. Effect of initial dye concentration

The effect of dye concentration on color removal efficiency by both BS-FeONPs and CS-FeONPs was studied in the range of 10–50 mg/L dye solution concentrations. Data revealed that dye removal efficiency by both nanomaterials featured higher uptake removal at low concentrations, where dye removal percentage drops with the increase in dye concentration reaching 86.40% in case of BS-FeONPs and 40.67% in the case of CS-FeONPs (Fig. 10); this may be due to the saturation of sorption sites on both nanomaterials as the concentration of the dye increases [71], results also indicated the higher efficiency of BS-FeONPs on colour removal at all dye concentrations, which might be related to the occurrence of more biosorption sites on BS-FeONPs surface available for dye binding compared with CS-FeONPs.

3.2.5. Adsorption characteristics

In adsorption systems, the determination of the maximum adsorption capacity and development of an equation that could be accurately used for design purposes and optimization of economical equipment is important. Langmuir and Freundlich models are among the most common isotherms that can be used for the description of solid–liquid sorption systems [5]. Linear regression analyses of these models and a comparison of their correlation coefficient (R^2) can be used for selection of the best fit isotherm. The Freundlich and Langmuir equations can be represented, respectively, as below [9,11]:

A linear form of the Langmuir isotherm equation can be described as follows:

$$\frac{C_e}{q_e} = \frac{1}{bQ} + \frac{C_e}{Q} \tag{3}$$

where Q is the maximum amount of adsorption (mg/g) and b is the adsorption equilibrium constant (L/mg).

Also, linear form of the Freundlich isotherm equation expression can be obtained by taking a logarithm:

$$\log q_e = \log K + \frac{1}{n}\log C_e \tag{4}$$

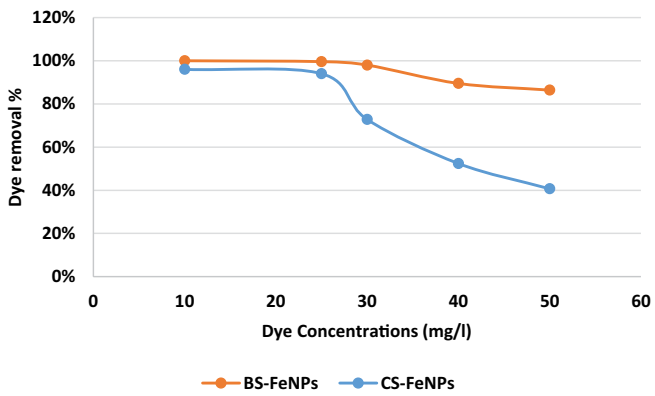

Fig. 10. Effect of initial dye concentration on color removal by BS-FeONPs and CS-FeONPs.

where C_e and q_e are parameters that are described in Eqs. (1) and (2). Constants k and n indicate the adsorption capacity and the adsorption intensity, respectively.

The parameters of Langmuir and Freundlich models were determined with plots of C_e vs. C_e/q_e and log q_e vs. log C_e. Application of the Langmuir and Freundlich models to the adsorption isotherm (Figs. 11–14) showed that the Langmuir isotherm model for both BS-FeONPs and CS-FeONPs turned out to be extremely satisfactory with the highest R^2 value (0.99), compared with Freundlich model.

The estimated values for the parameters of these models were shown in Tables 3 and 4. The essential feature of the Langmuir isotherm can be described with dimensionless separation factor or equilibrium constant R_L that is used for the description of the adsorption condition, which can be expressed as follows [9]:

$$R_L = \frac{1}{1 + bC_0} \tag{5}$$

where C_0 is the initial concentration of dye, the value of R_L represents the adsorption situations to be unfavorable ($R_L > 1$), linear ($R_L = 1$), favorable ($R_L < 1$) or irreversible ($R_L = 0$) [11]. Based on the Langmuir constant, the value of this parameter for MB adsorption on both BS-FeONPs and CS-FeONPs confirms that the adsorption of this dye with this material is irreversible under the conditions of this study. It could be derived that the Langmuir isotherm gave better fits than the other isotherm, where the maximum uptake capacity for MB is 29 mg/g with BS-FeONPs and 19.1 mg/g with CS-FeONPs.

3.2.6. Kinetic parameters of adsorption

The kinetics of dye adsorption onto both nano materials can be determined with different kinetic models. In this research, the kinetics of MB dye adsorption within BS-FeONPs and CS-FeONPs was evaluated with the pseudo-first-order and pseudo-second-order models (Figs. 15 and 16). For the analysis of data with the first model, the linear form of Lagergren equation was used, which can be expressed as follows:

$$\frac{dq_t}{dt} = K_1\left(q_e - q_t\right) \tag{6}$$

The integrated form of this equation can be written as follows:

$$\log\left(q_e - q_t\right) = \log\left(q_e\right)\frac{K_1}{2.203}t \tag{7}$$

where q_e and q_t are the amounts of dye adsorbed per unit weight of adsorbent (mg/g) at equilibrium time and time t, and K_1 is the rate constant for pseudo-first-order kinetics. The value of this constant has been calculated from the plot of log(q_e – q_t) vs. t. Several studies showed that the first-order model may not fully describe the adsorption kinetics; so in this study we used the pseudo-second-order equations. This model is often successfully used to describe

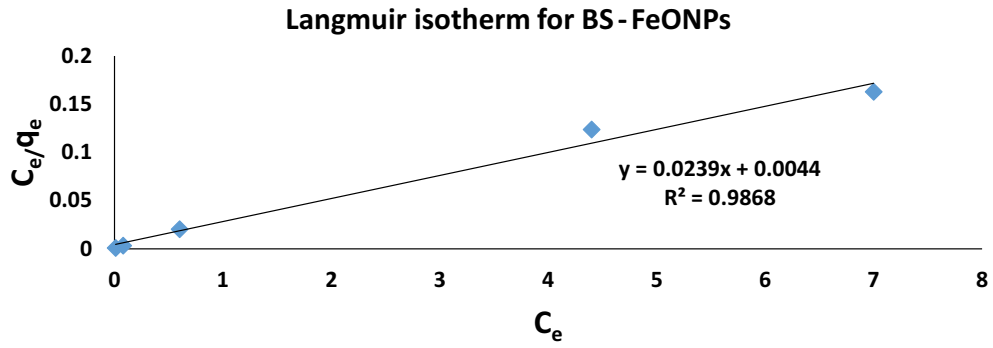

Fig. 11. Langmuir adsorption isotherm for biologically synthised nano iron oxide.

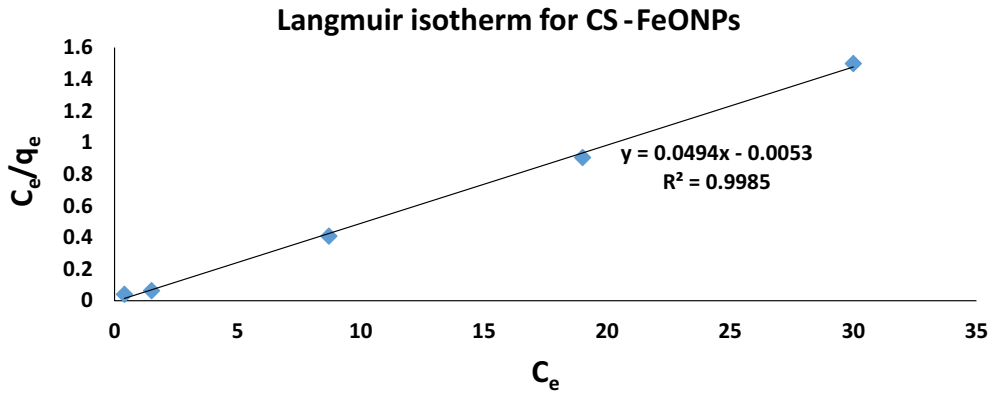

Fig. 12. Langmiur adsorption isotherm for chemically synthised nano iron oxide.

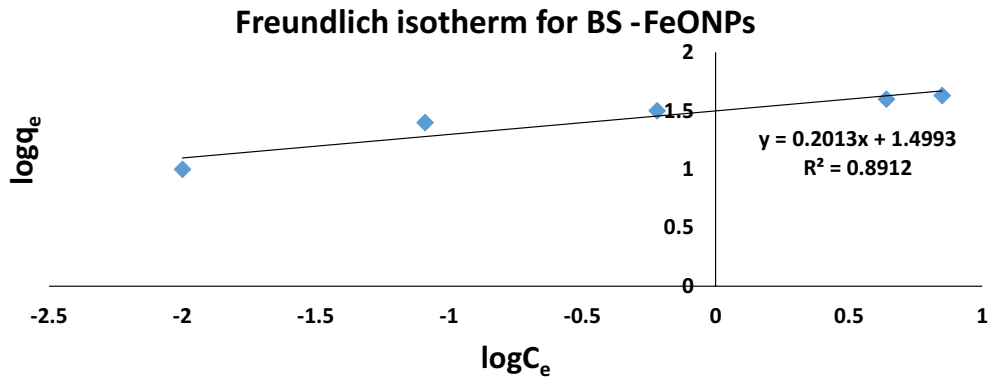

Fig. 13. Freundlich adsorption isotherm for biologically synthised nano iron oxide.

the kinetics of fixation reaction of adsorbate on adsorbent surface. The equation of this model can be described as follows:

$$\frac{dq_t}{dt} = K_2\left(q_e - q_t\right)^2 \tag{8}$$

The linear and integrated form can be expressed as follows:

$$\frac{t}{q_t} = \frac{1}{K_2 q_e^2} + \frac{1}{q_e}t \tag{9}$$

where K_2 is the rate constant of adsorption, q_e is the amount of MB adsorbed at equilibrium (mg/g) and q_t is the amount of dye adsorbed at time t (mg/g). The equilibrium adsorption capacity (q_e) and the rate constant K_2 (g/mg min) can be determined with the plot of t/q_t vs. t [13]. An analysis of data and regression coefficient (R^2) of Figs. 15 and 16 showed that the pseudo-first-order kinetic model does not fit well with the MB adsorption onto BS-FeONPs and CS-FeONPs (R^2 = 0.6 and 0.96) and the adsorption of this dye complies with the pseudo-second-order kinetics, because the correlation coefficient of this model is higher than 0.99, the calculated adsorption capacity complies with the experimental

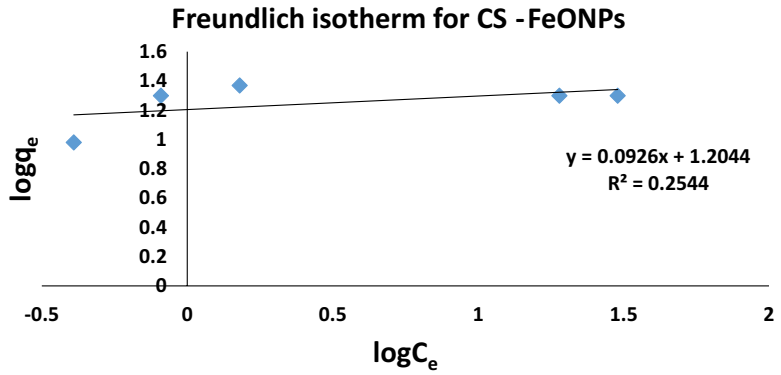

Fig. 14. Freundlich adsorption isotherm for chemically synthised nano iron oxide.

Table 3
Langmuir and Freundlich parameters for BS-FeONPs

	Langmuir		Freundlich	
BS-FeONPs	b (L/mg)	14.13	k (L/g)	1.25
	q_{max} (mg/g)	29.14	n	0.70
	R^2	0.98	R^2	0.89

Table 4
Langmuir and Freundlich parameters for CS-FeONPs

	Langmuir		Freundlich	
CS-FeONPs	b (L/mg)	110.10	k (L/g)	0.60
	q_{max}(mg/g)	19.08	n	0.80
	R^2	0.99	R^2	0.25

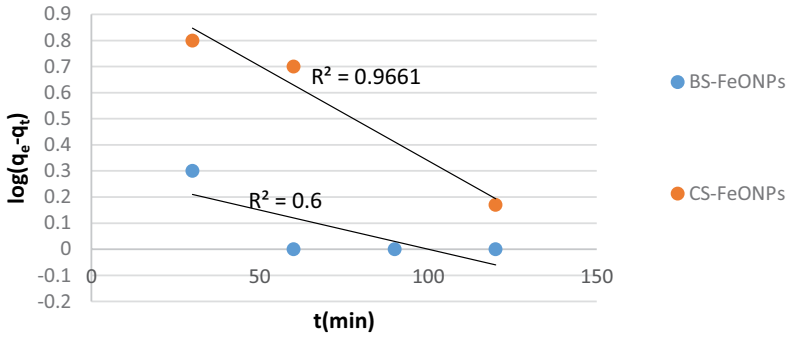

Fig. 15. Pseudo-first-order kinetics of MB adsorption onto FeONPs.

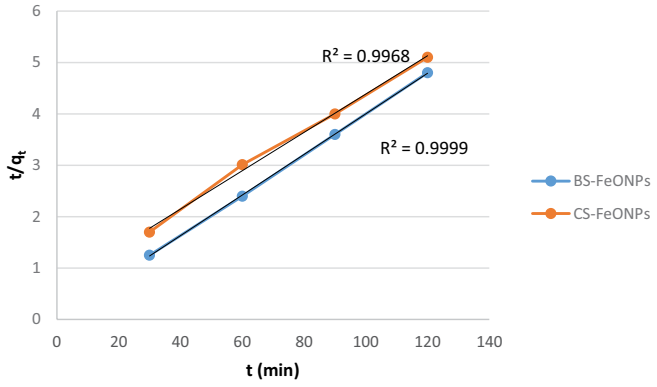

Fig. 16. Pseudo-second-order kinetics of MB adsorption onto FeONPs.

values. The values of K_1 and K_2 in case of BS-FeNOPs were calculated as 0.05 and 0.61 min^{-1} for pseudo-first-order and pseudo-second-order kinetics, respectively. The values of K_1 and K_2 in case of CS-FeNOPs were calculated as 0.02 and 0.43 min^{-1} for pseudo-first-order and pseudo-second-order kinetics, respectively.

3.3. Recovery and reuse of iron oxide nanoparticles

The recyclability of biologically and chemically synthesized iron oxide nanoparticles was evaluated after recovery; it was found that the catalytic activity of both BS-FeONPs and CS-FeONPs towards adsorption of methylene blue dye was retained with almost the same efficiency as previously mentioned in all experiments at optimum dose of 0.1 g where MB removal percentage was 99% after 60 min in case of BS-FeONPs and 94% in case of CS-FeONPs after 90 min (Fig. 17) at room temperature and pH 7. Our results found support from the study by Bhalkikar et al. [77] who evaluated recycling procedures of magnetite nanoparticles (Fe_3O_4 NPs) used to catalyze the one-pot conversion of cellobiose, a glucose disaccharide, to 5-hydroxymethylfurfural (5-HMF); they found that after recovery, and reusing of Fe_3O_4 NPs catalyst, it regained its activity with similar

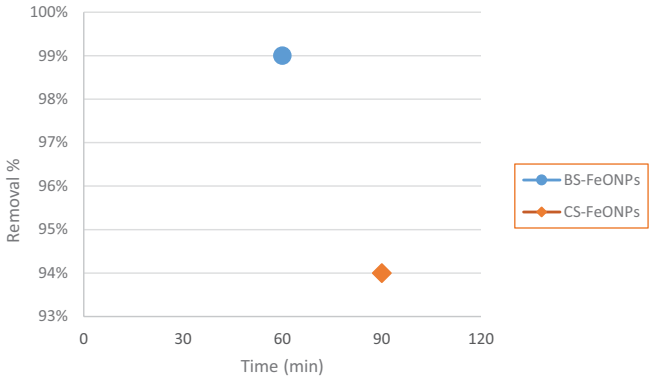

Fig. 17. Removal % of recovered BS-FeONPs and CS-FeONPs with respect to time.

5-HMF yields, in addition the XRD patterns of the Fe_3O_4 NPs after reusing remained similar to that before the reaction, revealing that Fe_3O_4 of the NP catalyst remained as the active component in all recycling experiments, where no changes into other forms of iron oxides was detected.

4. Conclusion

Characterization analyses of nanoparticles in present study reflected the higher adsorptive capacity of BS-FeONPs towards MB dye compared with CS-FeONPs, this was confirmed by results of adsorption experiments including effect of pH, contact time and dye concentration on dye removal efficiency. Adsorption data for both BS-FeONPs and CS-FeONPs complies with Langmuir isotherm equation model ($R^2 = 0.99$) and the maximum adsorption amount (q_{max}) was 29.14 and 19.08 mg/g for BS-FeONPs and CS-FeONPs, respectively. Kinetic studies revealed that the adsorption of MB is rapid and complies with the pseudo-second-order kinetic ($R^2 > 0.99$). Study also proved that adsorptive capacity of both synthesized nanomaterials was retained with almost the same efficiency after recovery indicating the availability of reusing studied nanoparticles in further dye removal applications, which was considered from economic point of view a promising future approach. A broad future research is recommended to improve the assembly of iron oxide nanoparticles from biological sources in order to increase degradation of environmental pollution with least eco-toxicological influences. Moreover, an inclusive risk assessment of green synthesis of FeONPs must be implemented to consider destiny, passage, dissolution and kinetics of these nanoparticles during processing and applications.

Acknowledgment

The authors would like to acknowledge Central Laboratory for Environmental Quality Monitoring (CLEQM), National Water Research Center (NWRC) for providing all possible facilities to conduct and complete this research.

References

[1] L.C. Arteagaa, M.P. Zavaletaa, W.M. Eustaquiob, J.M. Bobadilla, Removal of aniline blue dye using live microalgae *Chlorella vulgaris*, Energy Environ. Sci., 2 (2018) 6–12.
[2] M. Auta, B. Hameed, Preparation of waste tea activated carbon using potassium acetate as an activating agent for adsorption of Acid Blue 25 dye, Chem. Eng. J., 171 (2011) 502–509.
[3] V.K. Gupta, D. Pathania, S. Agarwal, P. Singh, Adsorptional photocatalytic degradation of methylene blue onto pectin–CuS nanocomposite under solar light, J. Hazard. Mater., 243 (2012) 179–186.
[4] Ö. Tunc, H. Tanacı, Z. Aksu, Potential use of cotton plant wastes for the removal of Remazol Black B reactive dye, J. Hazard. Mater., 163 (2009) 187–198.
[5] Y. Yang, G. Wang, B. Wang, Z. Li, X. Jia, Q. Zhou, Biosorption of Acid Black 172 and Congo Red from aqueous solution by nonviable Penicillium YW 01: kinetic study, equilibrium isotherm and artificial neural network modeling, Bioresour. Technol., 102 (2011) 828–834.
[6] S. Altenor, B. Carene, E. Emmanuel, J. Lambert, Adsorption studies of methylene blue and phenol onto vetiver roots activated carbon prepared by chemical activation, J. Hazard. Mater., 165 (2009) 1029–1039.
[7] Z. Aksu, Application of biosorption for the removal of organic pollutants: a review, Process Biochem., 40 (2005) 997–1026.
[8] Z. Aksu, S. Tezer, Biosorption of reactive dyes on the green alga *Chlorella vulgaris*, Process Biochem., 40 (2005) 1347–1361.
[9] R. Patel. S. Suresh, Kinetic and equilibrium studies on the biosorption of reactive black 5 dye by *Aspergillus foetidus*, Bioresour. Technol., 99 (2008) 51–58.
[10] A. Srinivasan, T. Viraraghavan, Decolorization of dye wastewaters by biosorbents: a review, J. Environ. Manage., 91 (2010) 1915–1929.
[11] M.E. Russo, F. Di Natale, V. Prigione, V. Tigini, A. Marzocchella, G.C. Varese, Adsorption of acid dyes on fungal biomass: equilibrium and kinetics characterization, Chem. Eng. J., 162 (2010) 537–545.
[12] A. Çelekli, F. Geyik, Artificial neural networks (ANN) approach for modeling of removal of Lanaset Red G on *Chara contraria*, Bioresour. Technol., 102 (2011) 5634–5638.
[13] G.L. Dotto, L.A.d.A. Pinto, Adsorption of food dyes onto chitosan: optimization process and kinetic, Carbohydr. Polym., 84 (2011) 231–238.
[14] H.Y. El-Kassas, L.A. Mohamed, Bioremediation of the textile waste effluent by *Chlorella vulgaris*, Egypt. J. Aquat. Res., 40 (2014) 301–308.
[15] A. Seker, T. Shahwan, A.E. Eroğlu, S. Yilmaz, Z. Demirel, M.C. Dalay, Equilibrium thermodynamic and kinetic studies for the biosorption of aqueous lead (II), cadmium (II) and nickel (II) ions on *Spirulina platensis*, J. Hazard. Mater., 154 (2008) 973–980.
[16] A. Çelekli, H. Bozkurt, Bio-sorption of cadmium and nickel ions using *Spirulina platensis*: kinetic and equilibrium studies, Desalination, 275 (2011) 141–147.
[17] L. Fang, C. Zhou, P. Cai, W. Chen, X. Rong, K. Dai, W. Liang, J. Gu, Q. Huang, Binding characteristics of copper and cadmium by cyanobacterium *Spirulina platensis*, J. Hazard. Mater., 190 (2011) 810–815.
[18] W. Cheung, Y. Szeto, G. McKay, Enhancing the adsorption capacities of acid dyes by chitosan nano particles, Bioresour. Technol., 100 (2009) 1143–1148.
[19] B.S. Inbaraj, B. Chen, Dye adsorption characteristics of magnetite nanoparticles coated with a biopolymer poly (γ-glutamic acid), Bioresour. Technol., 102 (2011) 8868–8876.
[20] D. Mandal, M.E. Bolander, D. Mukhopadhyay, G. Sarkar, P. Mukherjee, The use of microorganisms for the formation of metal nanoparticles and their application, Appl. Microbiol. Biotechnol., 69 (2006) 485–492.
[21] A. Jebali, F. Ramezani, B. Kazemi, Biosynthesis of silver nanoparticles by *Geotricum sp*, J. Clust. Sci., 22 (2011) 225–232.
[22] S. Saif, A. Tahir, Y. Chen, Green synthesis of iron nanoparticles and their environmental applications and implications, Nanomaterials, 6 (2016) 209.
[23] S. Siji, J. Njana, P. Amrita, D. Vishnudasan, Biogenic synthesis of iron oxide nanoparticles from marine algae, Int. J. Multidiscip. Res., 1 (2018) 1–7.

[24] M.F. Lengke, M.E. Fleet, G. Southam, Morphology of gold nanoparticles synthesized by filamentous cyanobacteria from gold (I)− thiosulfate and gold (III)− chloride complexes, Langmuir, 22 (2006) 2780–2787.
[25] G. Singaravelu, J. Arockiamary, V.G. Kumar, K. Govindaraju, A novel extracellular synthesis of monodisperse gold nanoparticles using marine alga, *Sargassum wightii* Greville, Colloids Surf. B, 57 (2007) 97–101.
[26] T. Ogi, N. Saitoh, T. Nomura, Y. Konishi, Room-temperature synthesis of gold nanoparticles and nanoplates using Shewanella algae cell extract, J. Nanopart. Res., 12 (2010) 2531–2539.
[27] A. Rahman, A. Ismail, D. Jumbianti, S. Magdalena, H. Sudrajat, Synthesis of copper oxide nano particles by using *Phormidium cyanobacterium*, Indonesian J. Chem., 9 (2009) 355–360.
[28] S. Honary, H. Barabadi, E. Gharaei-Fathabad, F. Naghibi, Green synthesis of copper oxide nanoparticles using *Penicillium aurantiogriseum*, *Penicillium citrinum* and *Penicillium waksmanii*, Dig. J. Nanomater. Biostruct., 7 (2012) 999–1005.
[29] W.J. Crookes-Goodson, J.M. Slocik, R.R. Naik, Bio-directed synthesis and assembly of nanomaterials, Chem. Soc. Rev., 37 (2008) 2403–2412.
[30] A.K. Gade, P. Bonde, A.P. Ingle, P.D. Marcato, N. Durán, M.K. Rai, Exploitation of *Aspergillus niger* for synthesis of silver nanoparticles, J. Biobased Mater. Bioenergy, 2 (2008) 243–247.
[31] C.K. Lee, S.S. Liu, L.C. Juang, C.C. Wang, M.D. Lyu, S.H. Hung, Application of titanate nanotubes for dyes adsorptive removal from aqueous solution, J. Hazard. Mater., 148 (2007) 756–760.
[32] R. Salehi, M. Arami, N.M. Mahmoodi, H. Bahrami, S. Khorramfar, Novel biocompatible composite (chitosan–zinc oxide nanoparticle): preparation, characterization and dye adsorption properties, Colloids Surf., B, 80 (2010) 86–93.
[33] X. Li, W. Xiao, G. He, W. Zheng, N. Yu, M. Tan, Pore size and surface area control of MgO nanostructures using a surfactant-templated hydrothermal process: high adsorption capability to azo dyes, Colloids Surf., A, 408 (2012) 79–86.
[34] C. Păcurariu, O. Paşka, R. Ianoş, S.G. Muntean, Effective removal of methylene blue from aqueous solution using a new magnetic iron oxide nanosorbent prepared by combustion synthesis, Clean Technol. Environ. Policy, 18 (2016) 705–715.
[35] T. Neuberger, B. Schöpf, H. Hofmann, M. Hofmann, B. Von Rechenberg, Superparamagnetic nanoparticles for biomedical applications: possibilities and limitations of a new drug delivery system, J. Magn. Magn. Mater., 293 (2005) 483–496.
[36] M. Mahdavi, F. Namvar, M.B. Ahmad, R. Mohamad, Green biosynthesis and characterization of magnetic iron oxide (Fe_3O_4) nanoparticles using seaweed (*Sargassum muticum*) aqueous extract, Molecules, 18 (2013) 5954–5964.
[37] H.Y. El-Kassas, M.A. Aly-Eldeen, S.M. Gharib, Green synthesis of iron oxide (Fe_3O_4) nanoparticles using two selected brown seaweeds: characterization and application for lead bioremediation, Acta Oceanol. Sinica, 35 (2016) 89–98.
[38] Y.P. Yew, K. Shameli, M. Miyake, N. Kuwano, N.B.B.A. Khairudin, S.E.B. Mohamad, K.X. Lee, Green synthesis of magnetite (Fe_3O_4) nanoparticles using seaweed (*Kappaphycus alvarezii*) extract, Nanoscale Res. Lett., 11 (2016) 276.
[39] S.L. Lim, W.L. Chu, S.M. Phang, Use of *Chlorella vulgaris* for bioremediation of textile wastewater, Bioresour. Technol., 101 (2010) 7314–7322.
[40] E. Acuner, F. Dilek, Treatment of tectilon yellow 2G by *Chlorella vulgaris*, Process Biochem., 39 (2004) 623–631.
[41] M. Hernández-Zamora, E. Cristiani-Urbina, F. Martínez-Jerónimo, H.V. Perales-Vela, T. Ponce-Noyola, M.C. Montes-Horcasitas, R.O. Cañizares-Villanueva, Bioremoval of the azo dye Congo Red by the microalga *Chlorella vulgaris*, Environ. Sci. Pollut. Res., 22 (2015) 10811–10823.
[42] S.Y. Mak, D.H. Chen, Fast adsorption of methylene blue on polyacrylic acid-bound iron oxide magnetic nanoparticles, Dyes Pigm., 61 (2004) 93–98.
[43] Y.T. Lin, C.H. Weng, F.Y. Chen, Effective removal of AB24 dye by nano/micro-size zero-valent iron, Sep. Purif. Technol., 64 (2008) 26–30.
[44] Z. Zhang, J. Kong, Novel magnetic Fe_3O_4@C nanoparticles as adsorbents for removal of organic dyes from aqueous solution, J. Hazard. Mater., 193 (2011) 325–329.
[45] T. Shahwan, S. Abu Sirriah, M. Nairat, E. Boyacı, A.E. Eroglu, T.B. Scott, K.R. Hallam, Green synthesis of iron nanoparticles and their application as a Fenton-like catalyst for the degradation of aqueous cationic and anionic dyes, Chem. Eng. J., 172 (2011) 258–266.
[46] J.S.T. Hernandez, A.A. Muriel, J. Tabares, G.P. Alcázar, A. Bolaños, Preparation of Fe_3O_4 nanoparticles and removal of methylene blue through adsorption, J. Phys. Conf. Ser., 614 (2015) 012007.
[47] S.H. Kim, P.P. Choi, Enhanced Congo red dye removal from aqueous solutions using iron nanoparticles: adsorption, kinetics, and equilibrium studies, Dalton Trans., 46 (2017) 15470–15479.
[48] I. Ali, C. Peng, Z.M. Khan, M. Sultan, I. Naz, Green synthesis of phytogenic magnetic nanoparticles and their applications in the adsorptive removal of crystal violet from aqueous solution, Arab. J. Sci. Eng., 43 (2018) 6245–6259.
[49] R.Y. Stanier, R. Kunisawa, M. Mandel, G. Cohen-Bazire, Purification and properties of unicellular blue-green algae (order Chroococcales), Bacteriol. Rev., 35 (1971) 171.
[50] F. Thema, P. Beukes, A. Gurib-Fakim, M. Maaza, Green synthesis of Monteponite CdO nanoparticles by *Agathosma betulina* natural extract, J. Alloys Compd., 646 (2015) 1043–1048.
[51] M.M.S.I. Khaleelullah, M. Murugan, K.V. Radha, D. Thiyagarajan, Y. Shimura, Y. Hayakawa, Synthesis of superparamagnetic iron oxide nanoparticles assisted by brown seaweed *Turbinaria decurrens* for removal of reactive navy blue dye, Mater. Res. Express, 4 (2017) 105038.
[52] T.S. Hui, M.A.A. Zaini, Isotherm studies of methylene blue adsorption onto potassium salts-modified textile sludge, J. Teknol., 74 (2015) 57–63.
[53] N. Efecan, T. Shahwan, A.E. Eroğlu, I. Lieberwirth, Characterization of the uptake of aqueous Ni2+ ions on nanoparticles of zero-valent iron (nZVI), Desalination, 249 (2009) 1048–1054.
[54] Y.P. Sun, X.Q. Li, W.X. Zhang, H.P. Wang, A method for the preparation of stable dispersion of zero-valent iron nanoparticles, Colloids Surf., A, 308 (2007) 60–66.
[55] Y.P. Yew, K. Shameli, M. Miyake, N.B.B.A. Khairudin, S.E.B. Mohamad, T. Naiki, K.X. Lee, Green biosynthesis of superparamagnetic magnetite Fe_3O_4 nanoparticles and biomedical applications in targeted anticancer drug delivery system: a review, Arab. J. Chem., 13 (2020) 2287–2308.
[56] D.K. Lee, Y.S. Kang, Preparation and characterization of magnetic nanoparticles by γ-irradiation, Mater. Sci. Eng. C, 24 (2004) 107–111.
[57] S. Siji, J. Njana, P.J. Amrita, A. Raj, D. Vishnudasan, M. Panicker, Green Synthesized Iron Nanoparticles and Its Uptake in *Pennisetum glaucum* — A Nanonutriomics Approach, in 2017 International Conference on Technological Advancements in Power and Energy (TAP Energy), (IEEE, 2017), pp. 1–8.
[58] A.S. Teja, P.Y. Koh, Synthesis, properties, and applications of magnetic iron oxide nanoparticles, Prog. Cryst. Growth Charact. Mater., 55 (2009) 22–45.
[59] Y. Lu, Y. Yin, B.T. Mayers, Y. Xia, Modifying the surface properties of superparamagnetic iron oxide nanoparticles through a sol− gel approach, Nano Lett., 2 (2002) 183–186.
[60] W. Wu, Q. He, C. Jiang, Magnetic iron oxide nanoparticles: synthesis and surface functionalization strategies, Nanoscale Res. Lett., 3 (2008) 397.
[61] S. Sun, H. Zeng, Size-controlled synthesis of magnetite nanoparticles, J. Am. Chem. Soc., 124 (2002) 8204–8205.
[62] N. Wang, L. Zhou, J. Guo, Q. Ye, J.M. Lin, J. Yuan, Adsorption of environmental pollutants using magnetic hybrid nanoparticles modified with β-cyclodextrin, Appl. Surf. Sci., 305 (2014) 267–273.
[63] E. Alp, N. Aydogan, A comparative study: synthesis of superparamagnetic iron oxide nanoparticles in air and N_2 atmosphere, Colloids Surf., A, 510 (2016) 205–212.

[64] S.L. Pal, U. Jana, P.K. Manna, G.P. Mohanta, R. Manavalan, Nanoparticle: an overview of preparation and characterization, J. Appl. Pharm. Sci., 1 (2011) 228–234.
[65] B. Kumar, K. Smita, L. Cumbal, A. Debut, S. Galeas, V.H. Guerrero, Phytosynthesis and photocatalytic activity of magnetite (Fe_3O_4) nanoparticles using the Andean blackberry leaf, Mater. Chem. Phys., 179 (2016) 310–315.
[66] V. Subramaniyam, S.R. Subashchandrabose, P. Thavamani, M. Megharaj, Z. Chen, R. Naidu Chlorococcum sp. MM11—a novel phyco-nanofactory for the synthesis of iron nanoparticles, J. Appl. Phycol., 27 (2015) 1861–1869.
[67] M.N. Nadagouda, A.B. Castle, R.C. Murdock, S.M. Hussain, R.S. Varma, In vitro biocompatibility of nanoscale zerovalent iron particles (NZVI) synthesized using tea polyphenols, Green Chem., 12 (2010) 114–122.
[68] M. Rahimi, Removal of methylene blue from wastewater by adsorption onto $ZnCl_2$ activated corn husk carbon equilibrium studies, J. Chem., 2013 (2013) 1–6.
[69] E. Alzahrani, Gum Arabic-coated magnetic nanoparticles for methylene blue removal, Int. J. Innov. Res. Sci. Eng. Technol., 3 (2014) 15118–15129.
[70] S. Senthilkumaar, P. Varadarajan, K. Porkodi, C. Subbhuraam, Adsorption of methylene blue onto jute fiber carbon: kinetics and equilibrium studies, J. Colloid Interface Sci., 284 (2005) 78–82.
[71] M. Mahmoud, Decolorization of certain reactive dye from aqueous solution using Baker's Yeast (*Saccharomyces cerevisiae*) strain, HBRC J., 12 (2016) 88–98.
[72] J. Ruana, I. Urbe, F. Borrull, Determination of phenols at the ng/l level in drinking and river waters by liquid chromatography with UV and electrochemical detection, J. Chromatogr. A, 655 (1993) 217–226.
[73] B.A. Fil, C. Ozmetin, M. Korkmaz, Cationic dye (methylene blue) removal from aqueous solution by montmorillonite, Bull. Korean Chem. Soc., 33 (2012) 3184–3190.
[74] T. Santhi, S. Manonmani, Adsorption of methylene blue from aqueous solution onto a waste aquacultural shell powders (Prawn Waste), Sustainable Environ. Res., 22 (2012) 45.
[75] Y. Özdemir, M. Doğan, M. Alkan, Adsorption of cationic dyes from aqueous solutions by sepiolite, Microporous Mesoporous Mater., 96 (2006) 419–427.
[76] M. Boumediene, H. Benaïssa, B. George, S. Molina, A. Merlin, Effects of pH and ionic strength on methylene blue removal from synthetic aqueous solutions by sorption onto orange peel and desorption study, J. Mater. Environ. Sci., 9 (2018) 1700–1711.
[77] A. Bhalkikar, Z.C. Gernhart, C.L. Cheung, Recyclable magnetite nanoparticle catalyst for one-pot conversion of cellobiose to 5-hydroxymethylfurfural in water, J. Nanomater., 2015 (2015) 1–8.